Third International Conference on CFD in the Minerals and Process Industries
CSIRO, Melbourne, Australia
10-12 December 2003

AN INVESTIGATION OF SPARGED MIXING TANKS USING ELECTRICAL IMPEDANCE TOMOGRAPHY AND COMPUTATIONAL FLUID DYNAMICS

Robert B. WHITE and Christian DOBLIN

CSIRO Minerals, Clayton, Victoria 3169, AUSTRALIA

ABSTRACT

A one metre diameter sparged mixing tank was fitted with an electrical imaging system and operated at six different operating conditions. Sparged mixing tanks are widely used in industry and it is relatively difficult to obtain measurements of gas dispersion during operation. This study investigates the performance of a Lightnin A310 in a gas sparged tank.

The results obtained using EIT were processed to provide time and spatial averages of electrical conductivity. Spatial averaging has been carried out in two stages: firstly radially at each measurement plane to produce five annular regions and also axially at six planes along the impeller shaft.

The corresponding CFD models provided steady-state values for volume fraction of air in the whole tank, and these results were processed to produce spatial averages for comparison.

This work has shown that it is possible to use electrical imaging techniques to investigate the gas dispersion in a sparged mixing tank and compare the results with those obtained from CFD models. Both sets of results compare well and can identify important trends in gas dispersion at the various operating conditions investigated.

INTRODUCTION

Commercial CFD codes available today can enable the rapid development of models of complex physical systems. The challenge for the engineer is to develop CFD models that represent the physical system with enough detail to provide some new insight to assist in the design process. Validation of the CFD models is therefore very important to give the engineer confidence in the model during the design process and also during plant optimisation activities.

This paper discusses some aspects of the on-going validation of a CFD model of a sparged mixing tank. Detailed measurements were made in a mixing tank using an electrical imaging system to obtain validation data at five different axial planes over a range of operating conditions. A three dimensional CFD model of the corresponding system was constructed and run at the corresponding operating conditions.

Electrical Impedance Tomography (EIT) has been used to obtain conductivity contours of a saline solution entering the surface of a mixing tank, Stanley et al, (2001). EIT data has successfully been used for the validation of CFD models in other conducting systems, such as a pipe reactor, White et al, (1999), and radial flow fixed bed reactor, Bolton et al., (2003). In the mixing tank and pipe reactor studies, the liquid tracer was a saline dye with relatively high conductivity. EIT could readily detect tracer-rich regions because of the difference in conductivity between the tracer and bulk fluid regions. The packing in the fixed bed reactor was non-conducting and EIT was well suited to track the locations of the conducting liquid.

Electrical tomographic techniques are not particularly well suited to identifying the presence of small features in large diameter vessels, even when there is a significant difference in electrical properties. Salem et al, (2001), report that the resolution of a 15 cm diameter copper sphere is acceptable near the wall but "grossly inferior" towards the centre of a 1.5 m diameter stirred tank filled with tap water. The copper sphere used in this study was hollow and weighted appropriately for neutral buoyancy.

EIT has often been used to track the movement of a tracer in the bulk fluid, and there is usually a significant difference in electrical conductivity between tracer and the bulk fluid. Researchers often use saline solutions as tracers, and the conductivity of the "tap water", "sea water" and "salty tap water" was found to be 87.7, 49000 and 53600 μS/cm, respectively, at 25°C, Chanson et al, (2002). (Where the salty tap water was made up of tap water and 3.45 wt% sodium chloride of 99.5% purity.)

Alternative measurement techniques are available to investigate sparged mixing tanks and the results have been used to validate CFD models. Power consumption of the motor driving the impeller and visual observations of gas hold up can be used as performance indicators, Otomo et al, (2003). Photographic techniques can be used to measure the drop sizes present during the mixing of immiscible liquids, Ok et al, (2003). Photographic techniques where the camera is mounted outside a transparent-walled vessel would be difficult to apply to a sparged mixing tank because of the high bubble concentration through the whole of the vessel. Laser based techniques, such as LDV and PIV, are better suited to optically transparent systems, but particle tracking techniques, such as those reported by Fishwick et al, (2003), have been used to monitor internal circulation rates and can provide similar velocity data that can be used for validation purposes.

MIXING TANK AND ELECTRICAL IMPEDANCE TOMOGRAPHY SYSTEM

The mixing vessel used in this study was one metre in diameter and was fitted with a 25 mm diameter air entry point at the centre of the base. Air flow was controlled using a linear rotameter and experiments were carried out at air flowrates of 50 and 100 % Full Scale, equivalent to

21.5 and 43 kg/h, respectively. Four axial baffles were fitted to the wall of the vessel and each baffle was 100 mm wide and 20 mm thick. The impeller shaft was 38 mm OD and the impeller was a 400 mm diameter Lightnin A310 that was positioned 220 mm from the bottom of the tank. Tests were carried out at 0 rpm, 120 rpm and 210 rpm.

The tank has walls 1.2 m tall and for these experiments the tank was filled to a level of 947 mm with tap water. The tank was equipped with 10 sensor planes to support tomography at intervals of 100mm between planes and 108 mm from the base of the tank to the bottom plane centre. Each sensor plane contained 16 equispaced sensors, and each sensor was 50 mm high by 100 mm wide.

The EIT system used in these experiments was a commercial ITS-2000 prototype tomographic processing module, manufactured by Industrial Tomography Systems (ITS). Images were reconstructed using software supplied on a commercial basis by ITS and is based on a non-iterative, linear back-projection technique. Reference tomograms comprising the average of ten measurements were obtained at each measurement location to ensure the series of 150 reconstructed images were of the highest quality.

In this study, a series of 150 reconstructed tomograms has been analysed to provide average conductivity readings for annular regions across several planes in the mixing tank. At each plane, the average conductivity has been determined in five internal regions, named A through E, where region A is the circular innermost region and regions B through E are annular. EIT results reported here are averages of planes 3 to 8, where plane 10 is the plane closest to the bottom of the tank. Results from the individual planes are not reported here because of space limitations.

The mixing tank is one meter in diameter and each annular region has a width of 100 mm. Four baffles fitted to the wall of the vessel are located in region E, each baffle is 100 mm wide and 20 mm thick. The inner region – region A - is circular with a radius of 100 mm and the 38 mm OD impeller shaft is at the centre of this region.

Measurement limitations

EIT is being used to infer the distribution of gas bubbles in water in this study. The conductivity of the tap water was 50 μS/cm at experimental conditions, and the conductivity of regions in the sparged mixing tank with a high concentration of bubbles was around 47 μS/cm. This is a particularly small difference in conductivity between the "tracer" – the region where gas bubbles occur – and the bulk fluid and a satisfactory relationship between conductivity and volume fraction of gas bubbles in water has not yet been determined. It is likely that the relationship between the conductivity and volume fraction of gas bubbles in water is non-linear because a relatively low resistance pathway exists through the water that surrounds the individual gas bubbles in the "measurement volume".

The introduction of gas into the liquid caused the free surface at the top of the tank to rise by up to 70 mm. The electric field around the top measurement planes was thus significantly changed between the reference state and measurement state, more so than any small change in the average liquid conductivity caused by the gas. As a consequence the tomographic measurements from the top two measurement planes were discarded.

An added complication is that the actual geometry of the "measurement volume" in the mixing tank is difficult to determine because there are internal fittings, such as the stirring shaft and baffles. These fittings have significantly different electrical properties than water and are likely to have an impact on the electric field that develops as part of the measurement process. The "sensitivity map" that is used by the tomographic reconstruction software to process the EIT measurements does not include these fittings so it is possible that the spatial accuracy of the results has been reduced.

The very real possibility that the "sensitivity map" is distorted because of physical arrangements in the mixing tank has long been recognised, Polydorides et al, (2001), and forms the basis of the push towards the utilisation of more advanced reconstruction techniques and measurements that recognise a three dimensional measurement volume. Engineers have successfully used electrical tomography to characterise three dimensional systems using a stacked series of thin, two dimensional measurement planes.

THE COMPUTATIONAL MODEL

The CFD model of the sparged mixing tank presented in this paper is a three-dimensional, two phase, Eulerian – Eulerian steady-state model. A characteristic bubble size of 3 mm has been used, which is a reasonable estimate for bubble size in a sparged mixing tank. The package used for the modelling is CFX 5.6, a commercial code produced by Ansys-CFX that utilises an unstructured mesh and a moving frame of reference to represent the impeller movement. The MFR mesh representing the impeller contained 239354 tetrahedrons and the mesh representing the tank contained 410097 tetrahedrons.

RESULTS

The results from the CFD model are in the most convenient form to present for each of the six experimental conditions, as shown in Figure 1 where isosurfaces are plotted to indicate the surface where the volume fraction of air is 2.5%. It can be seen that all flows are assymetrical and some key trends can be identified:

- At 0 rpm the rising gas plume is broader at 100% air flow than at 50% air flow, see Figure 1 A and B, respectively.
- The gas dispersion at 120 rpm and 50% air in the central region is nearly as extensive as the gas dispersion at 0 rpm and 100% air and there is some recirculation of gas at the surface, see Figure 1 C and B, respectively.
- At 120 rpm, the gas dispersion at 100% air is more extensive in the region mid-way along the shaft than at 50% air and there is no gas recirculation, see Figure 1 D and C, respectively.
- At 210 rpm, gas dispersion is greater at the bottom of the tank than at the top of the tank at 25% air flow, see Figure 1 E.

- The gas dispersion at 210 rpm and 100% air is most extensive in the central region and there is significant recirculation of gas from the surface, see Figure 1 F.

The qualitative "feel" that can be developed for the internal flow pattern by this type of comparison has been useful in interpreting the quantitative results obtained from the EIT investigation of corresponding operating conditions. Figure 2 shows the overall average conductivities measured in each radial region across the lowest six measurement planes in the axial direction.

It is possible to rank the performance of the sparged mixing tank at each operating condition by analysing the trends presented in Figure 2. The assumption made in the ranking process is that the average conductivity in a particular region decreases with volume fraction of air, but as yet a relationship between the volume fraction of air and average conductivity is not fully understood. It is also important to understand that the results shown in the figure relate to an overall average conductivity determined in each radial region at six planes in the axis of the tank generally above the impeller and beneath the free surface. The trend lines presented in Figure 2 indicate that:

- At 0 rpm, the average conductivity plot indicates that the rising gas plume at 50% air flow is bell shaped in the radial direction. Gas holdup appears to be significantly greater in region A than in region E, and the plot for 0 rpm and 0% air flow is included as a baseline.
- At 0 rpm and 100% air flow, the rising gas plume appears to be significantly broader in region A than at 50% air flow, which is consistent with the qualitative analysis of the CFD results, compare Figure 1 A and B.
- The rising gas plume at 210 rpm and 100% air flow appears to be the most extensive, as indicated by the bell shaped, average conductivity plot. Conductivities in all regions are significantly lower than at 0 rpm, 100% air flow - a reduction in average conductivity of 0.5 μS/cm at region E and 1.25 μS/cm at region A, compared to 0 rpm and 100 % air flow.
- The rising gas plume at 120 rpm and 100% air flow is not as extensive as that in the 210 rpm, 100% case, but follows a very similar form. Conductivities in all regions are roughly midway between the 0 rpm, 100% air flow case and the 210 rpm, 100% air flow case.
- At 210 rpm and 25% air flow, the average conductivity plot appears significantly "flatter", indicating that more gas holdup is occurring in regions beyond the centre of the tank. This indication is consistent with the qualitative analysis of the CFD results, see Figure 1 E, although the asymmetry in the axial gas dispersion cannot be resolved using this analysis technique.
- At 120 rpm and 50% air flow, a greater proportion of gas appears to be present in region E. The qualitative analysis of the CFD results, see Figure 1 C, identified that some gas re-entrainment from the surface was occurring.

The quantitative results showing average conductivity in each region obtained using the EIT have been compared with results from the CFD models. Figure 3 shows the average volume fraction of air that has been calculated for corresponding regions using results from the CFD runs.

The comparison of trend lines for average volume fraction of air and for average conductivity, Figure 3 and Figure 2, respectively, has identified some quite striking similarities in behaviour. The trend lines identified in Figure 3 show that:

- At 0 rpm, gas dispersion is greater at 100 % air flow than at 50 % air flow, as expected.
- At 100% air flow, the rising gas plume at 210 rpm provides more extensive gas dispersion than at 120 rpm.
- It is very interesting that the trend lines for 0 rpm, 50% and 100% airflow, and 100% air flow, 120 rpm and 210 rpm, are generally the same form, as noted in the analysis of the average conductivity plots.
- The trend line at 210 rpm and 25% air flow plot appears significantly "flatter" than the other cases reported here, indicating a higher proportion of gas in regions adjacent to the centre of the vessel. This indication is consistent with the quantitative analysis of the EIT results,
- The trend line at 120 rpm and 50% air flow indicates that more gas is present in the outer regions than expected, as noted earlier in the analysis of the average conductivity plots.

The results of CFD models can readily be represented as contour plots showing the volume fraction of air and vector plots showing the velocity of water at an axial-radial plane through the centre line of the vessel, see Figure 4 and Figure 5, respectively. Plots of this type can assist in characterising internal flow:

- At 0 rpm and 100% air flow, the high volume fraction of air in the centre of the vessel is clearly visible, see Figure 4 A, and confirms the trend line shown in Figure 3. The velocity vectors, see Figure 5 A, confirm that the rising gas plume establishes a flow pattern in the water with downward flow at the walls and upward flow in the centre regions.
- At 210 rpm and 25% air flow, gas hold up can be seen to occur low in the tank and to extend beyond the centre of the tank, see Figure 4 B, and is consistent with earlier interpretations. The velocity vectors, see Figure 5 B, confirm the downward pumping action of the impeller.
- At 210 rpm and 100% air flow, an extensive plume of rising gas is clearly visible, see Figure 4 C, which is consistent with earlier interpretations. The velocity vectors, see Figure 5 C, indicate that impeller is not operating effectively and the circulation pattern more closely resembles that of the gas driven system, see Figure 5 A.

CONCLUSION

This work has shown that it is possible to use electrical imaging techniques to investigate the gas dispersion in a sparged mixing tank and compare the results with those obtained from CFD models.

The results obtained using EIT were processed to provide time and spatial averages of electrical conductivity. The spatial averaging was carried out in two stages: firstly radially at each measurement plane to produce five annular regions and also axially at six planes along the impellor shaft.

The corresponding CFD models provided steady-state values for volume fraction of air in the whole tank, and these results were processed to produce spatial averages for comparison.

Both sets of results compare well and can identify important trends in gas dispersion at the various operating conditions investigated. A more detailed investigation to compare performance at each plane is currently being undertaken.

Analysis of contour plots showing volume fraction of air and vector plots showing water velocity, obtained by analysing the results of the CFD models, provide useful insight into the performance of the sparged mixing tank.

It should be pointed out that of the operating conditions investigated, the impeller could only be considered to be operating effectively at one condition, namely 210 rpm and 25% air flow. This condition would also have been identified if an analysis of power consumption had been undertaken.

Possible future work includes a similar type of analysis to be carried out comparing EIT and CFD results at each of the six axial planes, and also investigating the performance of a six-bladed Rushton impeller in similar operating conditions.

ACKNOWLEDGEMENTS

The authors would like to thank Jakub Bujalski, Graeme Lane and Darrin Stephens for interesting discussions about using CFD to model mixing tanks and to Kosta Simic for discussions regarding EIT.

REFERENCES

BOLTON, G.T., HOOPER, C.W., MANN, R. and STITT, E.H., (2003), "Flow distribution measurement in a radial flow fixed bed reactor using electrical resistance tomography", 3rd World Congress on Industrial Process Tomography, Banff, Canada.

CHANSON, H., AOKI, S. and HOQUE, A., (2002), "Scaling bubble entrainment and dispersion in vertical circular plunging jet flows: freshwater versus seawater", Proc. 5th International Conference on Hydrodynamics ICHD2002, pp 431-436, Tainan, Taiwan.

FISHWICK, R.P., STITT, E.H. and WINTERBOTTOM, J.M., (2003), "Study of stirred tank reactor hydrodynamics using prositron emission particle tracking", 3rd World Congress on Industrial Process Tomography, Banff, Canada.

OK, T., OOKOWARA, S., YOSHIKAWA, S. and OGAWA, K., "2003", "Drop size distribution in Liquid-liquid mixing", Journal of Chemical Engineering of Japan, Vol 36, No 8, pp 940-945.

OTOMO, N., BUJALSKI, W., NIENOW, A.W. and TAKAHASHI, K., (2003), "Gassed power consumption and gas hold-up for a dual hollow blade impeller system in a stirred vessel", Journal of Chemical Engineering of Japan, Vol 36, No 8, pp 905-911.

POLYDORIDES, N., LIONHEART, W.R. and MCCANN, H., (2001), "Considerations in Electrical Impedence Imaging", 2nd World Congress on Industrial Process Tomography, pp 367-394, Hannover, Germany.

SALEM, K., KLING, K., and MANN, R., (2001), "Application of Electrical Resistance Tomography (ERT) to monitor a flow-follower in a stirred tank", 2nd World Congress on Industrial Process Tomography, pp 159-167, Hannover, Germany.

STANLEY, S.J., WABO, E.L., MANN, R. and PRIMROSE, K., (2001), "Dual-validation of miscible liquid mixing in a stirred vessel imaged by electrical resistance tomography (ERT)", 2nd World Congress on Industrial Process Tomography, pp 151-158, Hannover, Germany.

WHITE, R.B., SIMIC, K. and STRODE, P., (2001), "The combined use of flow visualisation, Electrical Resistance Tomography and Computational Fluid Dynamics modelling to study mixing in a pipe", 2nd World Congress on Industrial Process Tomography, Hannover, Germany.

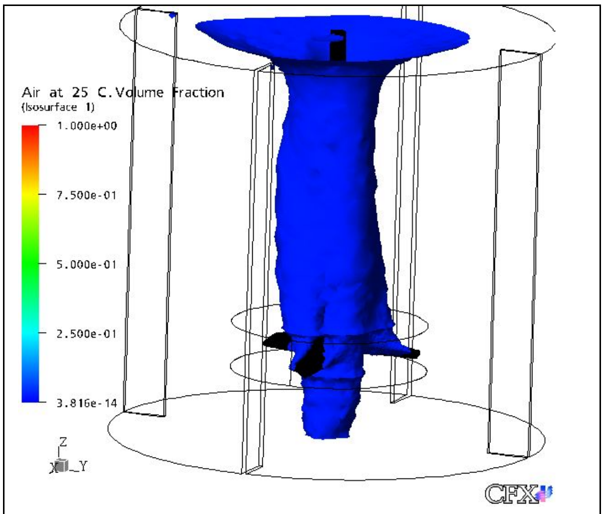

A 0 rpm 50% air

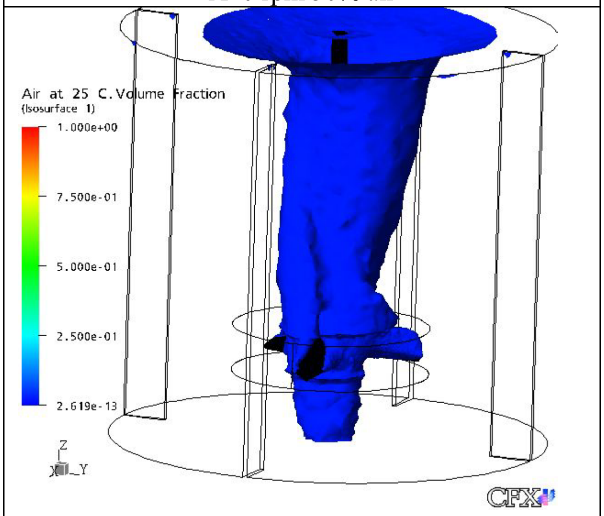

B 0 rpm 100% air

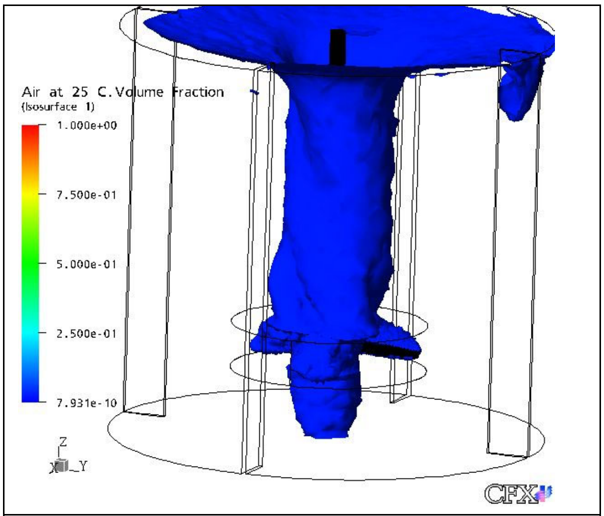

C 120 rpm 50% air downward pumping

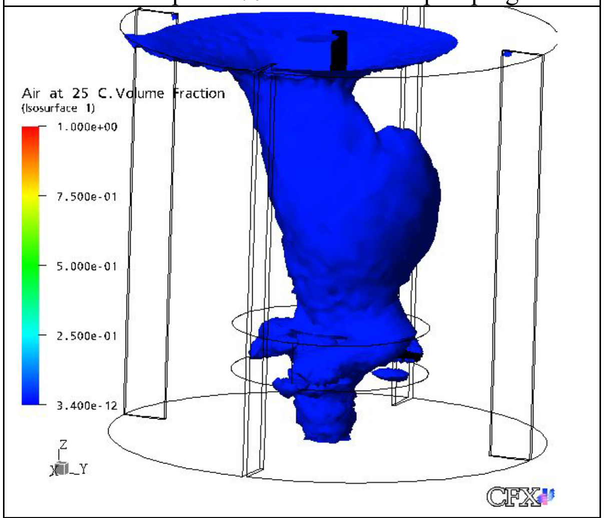

D 120 rpm 100% air downward pumping

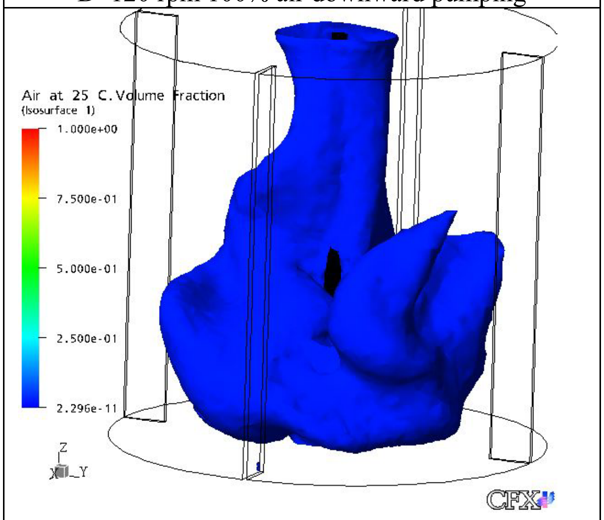

E 210 rpm 25% air downward pumping

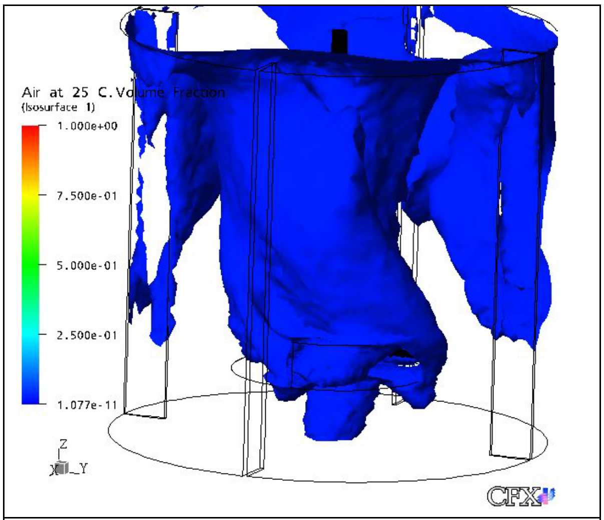

F 210 rpm 100% air downward pumping

Figure 1: Plots showing isosurfaces at 2.5% volume fraction of air for each test condition.

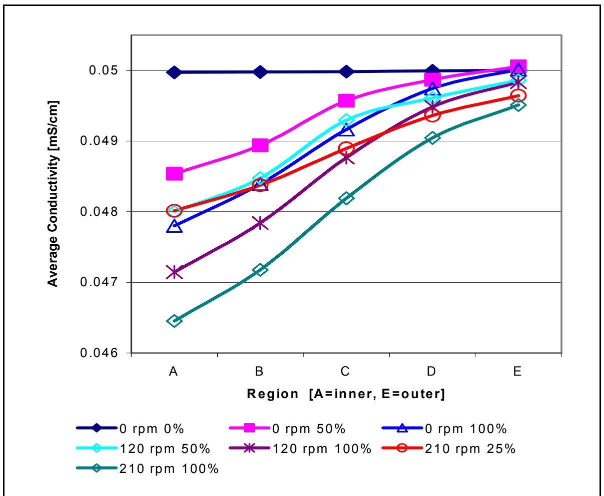

Figure 2: Plots showing overall average conductivity measured in each region at each test condition.

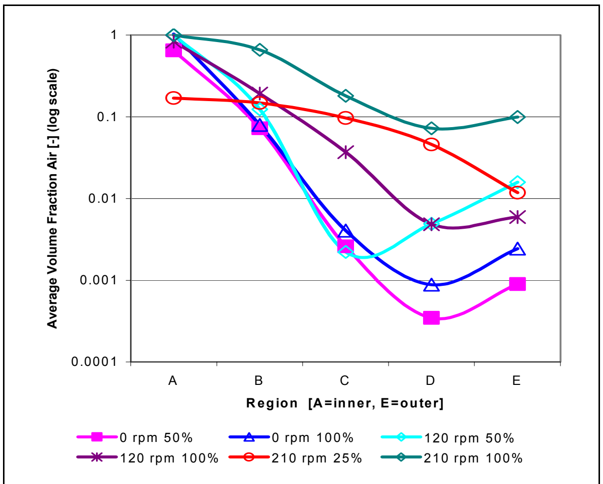

Figure 3: Plots showing overall average volume fraction of air in each region at each test condition.

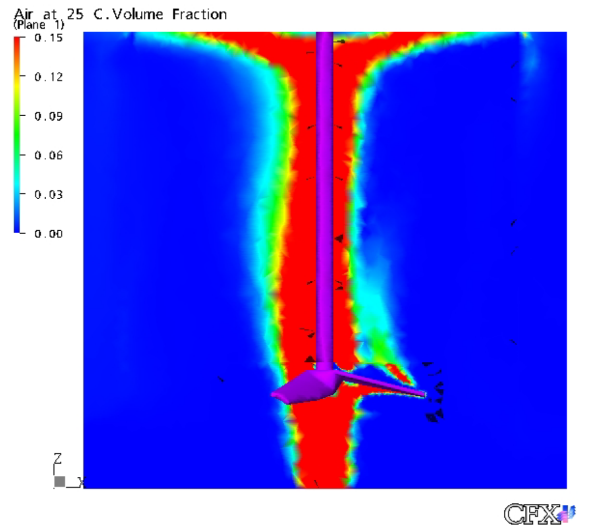

A 0 rpm 100% air

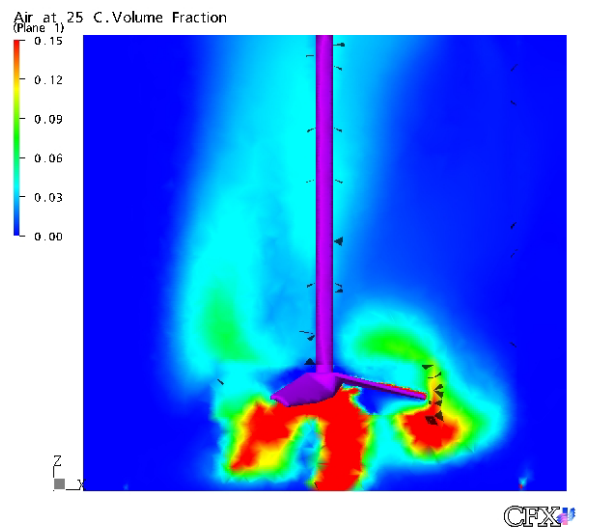

B 210 rpm 25% air downward pumping

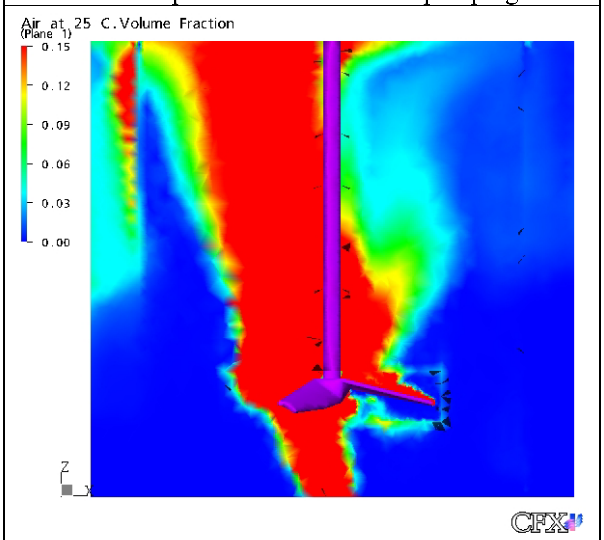

C 210 rpm 100% air downward pumping

Figure 4: Contour plots showing volume fraction of air at at 100% at 0 rpm, and 25% and 100% airflow at 210 rpm.

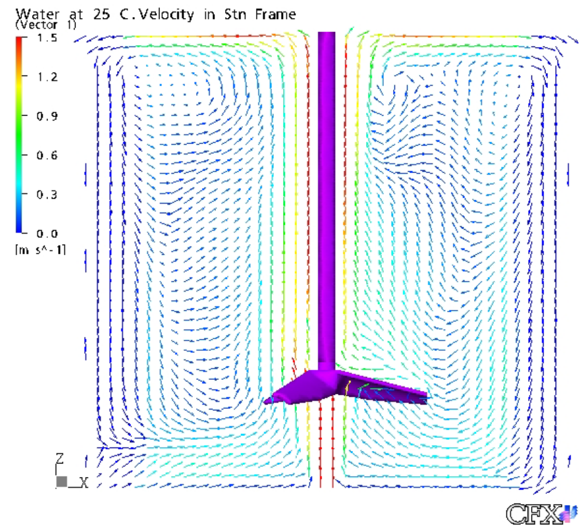

A 0 rpm 100% air

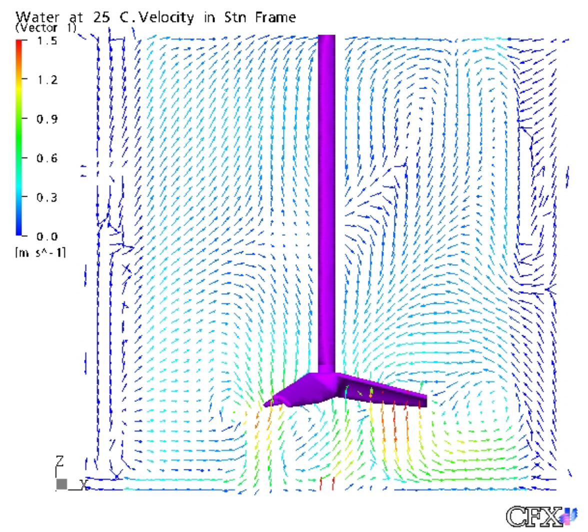

B 210 rpm 25% air downward pumping

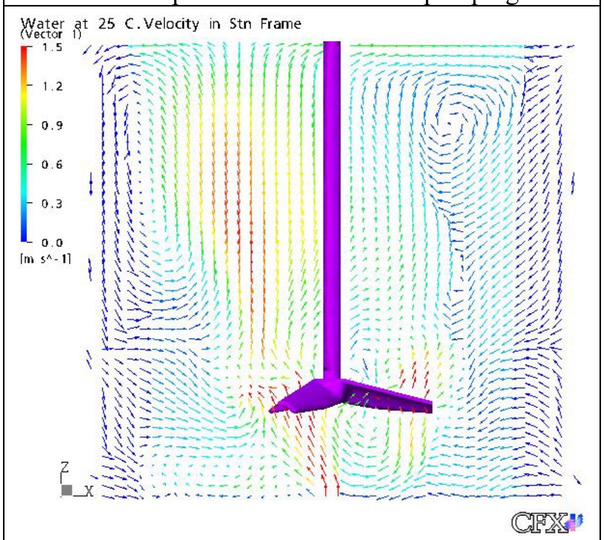

C 210 rpm 100% air downward pumping

Figure 5: Contour plots showing velocity vectors for water at 100% at 0 rpm, and 25% and 100% airflow at 210 rpm.